atmosphere

MDPI

Perspective

Advances in High-Resolution Spatiotemporal Monitoring Techniques for Indoor $PM_{2.5}$ Distribution

Qingyang Liu

College of Environment and Ecology, Nanjing Forestry University, Nanjing 210037, China; qyliu@njfu.edu.cn

Abstract

Indoor air pollution, including fine particulate matter ($PM_{2.5}$), poses a severe threat to human health. Due to the diverse sources of indoor $PM_{2.5}$ and its high spatial heterogeneity in distribution, traditional single-point fixed monitoring fails to accurately reflect the actual human exposure level. In recent years, the development of high spatiotemporal resolution monitoring technologies has provided a new perspective for revealing the dynamic distribution patterns of indoor $PM_{2.5}$. This study discusses two cutting-edge monitoring strategies: (1) mobile monitoring technology based on Indoor Positioning Systems (IPS) and portable sensors, which maps 2D exposure trajectories and concentration fields by having personnel carry sensors while moving; and (2) 3D dynamic monitoring technology based on in situ Lateral Scattering LiDAR (I-LiDAR), which non-intrusively reconstructs the 3D dynamic distribution of $PM_{2.5}$ concentrations using laser arrays. This study elaborates on the principles, calibration methods, application cases, advantages, and disadvantages of the two technologies, compares their applicable scenarios, and outlines future research directions in multi-technology integration, intelligent calibration, and public health applications. It aims to provide a theoretical basis and technical reference for the accurate assessment of indoor air quality and the prevention and control of health risks.

Keywords: $PM_{2.5}$; indoor air pollution; spatial distribution; mobile monitoring; 3D LiDAR; exposure assessment; spatiotemporal resolution

check for updates

Academic Editor: An-Soo Jang

Received: 9 September 2025
Revised: 14 October 2025
Accepted: 16 October 2025
Published: 17 October 2025

Citation: Liu, Q. Advances in High-Resolution Spatiotemporal Monitoring Techniques for Indoor $PM_{2.5}$ Distribution. *Atmosphere* **2025**, *16*, 1196. https://doi.org/10.3390/atmos16101196

Copyright: © 2025 by the author. Licensee MDPI, Basel, Switzerland. This article is an open access article distributed under the terms and conditions of the Creative Commons Attribution (CC BY) license (https://creativecommons.org/licenses/by/4.0/).

1. Introduction

The World Health Organization (WHO) has explicitly identified air pollution as the largest environmental health risk globally, with the number of premature deaths caused by it each year far exceeding other environment-related factors [1]. Among air pollutants, fine particulate matter with an aerodynamic diameter of $\leq$2.5 μm ($PM_{2.5}$) has become a key pollutant threatening human health due to its unique physicochemical properties [2]. Epidemiological studies have consistently linked $PM_{2.5}$ exposure to adverse health outcomes, including respiratory and cardiovascular diseases [3–7]. For instance, long-term exposure to elevated indoor $PM_{2.5}$ levels has been associated with significantly increased risks of chronic obstructive pulmonary disease and asthma [5]. These health impacts underscore the necessity for accurate exposure assessment, which is hindered by the limitations of traditional monitoring methods. Moreover, the International Agency for Research on Cancer (IARC) has classified outdoor $PM_{2.5}$ as a Group 1 carcinogen [8].

Humans spend approximately 80–90% of their time indoors, including in residences, offices, schools, and shopping malls [9]. The activity patterns of human show that indoor

air quality contributes more to the total human pollutant exposure than the outdoor environment [10]. For instance, in areas with low outdoor $PM_{2.5}$ concentrations, if indoor pollution sources such as cooking, smoking, or mosquito coil burning exist, exposure to $PM_{2.5}$ for human may remain high [11]. Conversely, when outdoor pollution is severe, the infiltration of outdoor air through building envelopes can significantly increase indoor $PM_{2.5}$ concentrations, resulting in a superposition effect of indoor pollution [12]. According to the Exposure Factors Handbook of Chinese Population (Adults) issued by China's Ministry of Environmental Protection (2013) [13], Chinese adults spend approximately 20–22 h per day indoors, accounting for 83–92% of their daily time. Even among adolescents, who generally spend more time outdoors, indoor occupancy exceeds 75% [13]. These findings underscore that personal exposure to $PM_{2.5}$ is largely determined by indoor concentrations rather than outdoor levels [14].

The sources of indoor $PM_{2.5}$ are highly complex and can be categorized into two types, which are outdoor infiltration and indoor primary emissions [15]. Outdoor infiltration primarily occurs through building gaps (e.g., around doors and windows) and ventilation systems, with its contribution ratio influenced by factors such as outdoor $PM_{2.5}$ concentrations, building airtightness, and ventilation methods [16]. Indoor primary emission sources are more widespread and dynamic, including cooking activities, tobacco combustion, combustion-related processes, cleaning and daily activities, and secondary fine particles generated by photochemical reactions of volatile organic compounds (VOCs) released from furniture and building materials [17,18]. These emission sources typically exhibit characteristics of point sources, transience, and high intensity, leading to strong spatial and temporal heterogeneity in indoor $PM_{2.5}$ concentrations [19]. For example, $PM_{2.5}$ concentrations near kitchen stoves may be 10–100 times higher than those in living room sofa areas; after smoking ceases, concentrations can decrease rapidly within minutes to tens of minutes, forming a significant temporal gradient [19].

Traditional monitoring methods of indoor air quality mostly rely on single-point or limited-point sensors installed at fixed heights (i.e., Eulerian approach) [20]. Although this approach can obtain time-series concentration data at specific monitoring points and support the assessment of long-term average pollution levels, it has significant limitations [11,19,21]. It cannot capture concentration gradients across the entire indoor space, making it difficult to identify pollution hotspots (e.g., hidden smoke sources) and clean areas with lower $PM_{2.5}$ concentrations, which easily leads to underestimation or overestimation of the actual exposure level when personnel move indoors [11,19,21]. Moreover, for transient or sudden pollution sources (e.g., short-term cooking or perfume spraying), fixed-point monitoring may miss critical data if not located along the pollution diffusion path [11,19,21]. Additionally, single-point monitoring cannot establish a correlation between pollutant concentrations and personnel activity trajectories, making it impossible to answer the core question of the personal $PM_{2.5}$ concentration. This limitation results in large deviations in health risk assessment [11,19,21].

Therefore, the development and application of monitoring technologies (i.e., Lagrangian approach) capable of capturing the spatial distribution of $PM_{2.5}$ with high resolution are crucial for accurately identifying pollution sources, understanding pollutant diffusion patterns, assessing actual human exposure, and formulating effective ventilation and purification strategies [11,22]. This study aims to discuss early advancements and identify research gaps that motivate the current technological innovations. The primary objective of this paper is to evaluate and compare two emerging high-resolution spatiotemporal monitoring approaches including mobile sensor-based and 3D LiDAR-based systems to highlight their principles, applications, and integration potential [11,19]. The innovation of this work lies in its comprehensive side-by-side

analysis of Lagrangian and Eulerian monitoring paradigms, proposing a synergistic framework that combines personal exposure tracking with full-field visualization to achieve multi-scale air quality assessment, which has not been systematically addressed in earlier literature.

2. Methods

To systematically understand the recent advances in high-resolution spatiotemporal monitoring techniques for indoor $PM_{2.5}$, a comprehensive literature review was conducted across Web of Science, Scopus, and PubMed using keywords including "indoor $PM_{2.5}$", "spatial monitoring", "mobile monitoring", "3D LiDAR", "exposure assessment", and "sensor network". The search covered publications from 2010 to 2024, with a focus on emerging technologies beyond traditional fixed-point monitoring. This review and analysis were conducted between January and March 2025, encompassing literature published up to December 2024. While the review draws notably on Cheng et al. (2019) [11] and He et al. (2022) [19] for detailed case analyses, it also integrates findings from over 30 key studies to provide a broader perspective on technological trends, comparative advantages, and integration potential.

3. Results and Discussion

3.1. Mobile Monitoring Technologywith Indoor Positioning and Portable Sensors

The core concept of mobile monitoring technology is to use personnel as mobile sensing nodes by having them carry portable sensors while moving [11,23]. These nodes continuously record geographic location information and real-time $PM_{2.5}$ concentration data along daily activity trajectories, establishing a precise correlation between time, location, and concentration. Compared with traditional fixed-point monitoring, this method more authentically reflects actual human exposure during indoor movement. It is particularly effective in identifying microenvironments that cause short-term peak exposures, thereby providing essential micro-scale data support for analyzing indoor $PM_{2.5}$ exposure risks. A typical implementation of this approach can be found in the work of Cheng et al. (2019), whodeveloped an integrated indoor $PM_{2.5}$ mobile monitoring system consisting of three core components: a portable $PM_{2.5}$ sensor module, a high-precision Indoor Positioning System (IPS), and a data synchronization and integration platform [11].

The sensor module employed a dual-sensor strategy, collocating a research-grade TSI SidePak AM510 with a low-cost Plantower PTSQ1005 unit to balance accuracy and cost. The positioning system utilized Marvelmind ultrasonic beacons, which comprised multiple stationary beacons deployed in the environment and a mobile beacon carried by the user, to achieve centimeter-level accuracy [11]. A central data platform, leveraging a Python3.6+-based server, synchronized the $PM_{2.5}$ measurements from the sensors with the real-time location data from the beacons [11].

These components work synergistically to achieve synchronous collection and fusion of $PM_{2.5}$ concentration and spatial location data (Figure 1).

The sensor module employs a dual-sensor strategy pairing a research-grade sensor with a low-cost alternative to balance accuracy and budgetary constraints(Figure 1). The TSI SidePak AM510, a research-grade device, uses light scattering photometry to measure mass concentration, offering high measurement accuracy (error $\leq \pm 10\%$) and a rapid response time (T90 $\leq$ 2 s), making it capable of capturing transient pollution events effectively (Table 1) [11]. Its sampling inlet is positioned at breathing zone height to simulate real human exposure. In contrast, the low-cost Plantower PTQS1005 is based on laser scattering principles, is compact, energy-efficient, and costs only 1/50 to 1/100 of the

SidePak. The Low-Cost Sensor (LCS) measurements were compared against the TSI SidePak AM510 as a reference instrument through collocated calibration experiments. Source-specific scaling factors (e.g., 1.8 for cooking, 2.3 for e-cigarette emissions) were derived to correct LCS readings, ensuring data accuracy under varying emission conditions [11]. Integrated with an ESP32 development board, it enables wireless data transmission via Wi-Fi, allowing scalable deployment (Table 1) [11]. By collocating the two sensors, data comparability is ensured through using the high-accuracy device as a benchmark to validate the performance of the low-cost sensor, which can offer flexibility for studies with varying resource constraints.



Figure 1. Schematic of the mobile $PM_{2.5}$monitoring system integrating portable sensors and indoor positioning beacons (as indicated by the yellow circles). Detailed system configuration is described in Section 2. (Adapted from Cheng et al., 2019 [11]; Copyright 2019 American Chemical Society).

Table 1. Key specifications of the representative sensors used in mobile monitoring systems [11].

Sensor Type	Accuracy	Response Time (T90)	Cost Range	Key Features
TSI SidePak AM510	$\leq \pm 10\%$	≤ 2 s	High (Research-grade)	Laser photometry, high accuracy
Plantower PTSQ1005	Varies by source	~10 s	Low (1/50–1/100 of SidePak)	Laser scattering, compact, Wi-Fi enabled

The positioning system utilizes Marvelmind ultrasonic beacons (915 MHz version 4.9) to achieve centimeter-level accuracy (± 2 cm) [11,24]. Twelve stationary beacons(fixed ultrasonic transmitters) are deployed at heights of 2–2.2 m near room corners and passageways to minimize signal obstruction, while one mobile beacon is carried by the user. The TSI SidePak AM510 sensor is worn by the user to measure $PM_{2.5}$ concentrations at breathing height. The system operates at an update rate of 16 Hz, with trajectory data output at 1 Hz after averaging [11]. The working principle involves the mobile beacon emitting

ultrasonic signals, which are received by multiple stationary beacons. Using Time-of-Flight (ToF) measurements, the system performs trilateration to determine the precise location of the mobile beacon [11]. Compared to Wi-Fi or Bluetooth-based systems that typically offer meter-level accuracy, this ultrasonic IPS provides superior spatial resolution, enabling accurate identification of microenvironments such as cooking stoves, desks, and other localized emission sources.

A Python-based data platform serves as the central hub for multi-source data synchronization and fusion [11]. It employs a high-precision clock for timestamp unification, aligns location and $PM_{2.5}$ measurements temporally, and structures the output into a time-coordinate-concentration data series stored in a file. The platform also performs outlier detection and processes over-threshold values (e.g., replacing maxed-out SidePak readings with 20 $\mu g/m^3$). This integrated system effectively identifies $PM_{2.5}$ concentration peaks and their spatial distributions resulting from activities such as cooking, smoking, and chemical spraying. By generating color-mapped trajectory plots, it visually highlights high-concentration zones (e.g., near stoves or smoking areas) and reveals dynamic pollution dispersion paths.

This mobile monitoring approach offers three significant advantages, which are high spatial flexibility, direct personal exposure assessment, and controllable operational cost [11]. It can cover microenvironments inaccessible to fixed sensors and provides a realistic representation of human exposure. However, several challenges remain. Low-cost sensors like the PTQS1005 exhibit source-dependent response variations and delayed response times (T90 $\approx$ 10 s), necessitating controlled experiments in well-mixed chambers to determine source-specific scaling factors (e.g., 1.8 for cooking and 2.3 for e-cigarette emissions) and the application of dynamic response compensation techniques such as first-order model deconvolution. Furthermore, the walking path of the user influences spatial representativeness, requiring a combination of random walking and intentional lingering near suspected sources. Carrying the sensing device may also interfere with natural movement and perturb local airflow [24]. To enhance data accuracy, several calibration strategies are adopted [25–27]. These include source-specific scaling factors, dynamic response compensation, real-time correction using a fixed SidePak as an on-site reference, and background concentration subtraction to account for baseline drift and outdoor infiltration [25–27]. These measures collectively significantly improve data reliability, making mobile monitoring an effective tool for assessing personal exposure and pinpointing pollution sources.

3.2. Three-Dimensional I-LiDAR Monitoring

The laser array is composed of 18 individual laser modules, each emitting a continuous-wave laser beam at a wavelength of 532 nm ($\pm$10 nm), with an output power ranging from 130 to 160 mW [19,28,29]. These lasers are classified as Class IIIB, necessitating strict safety protocols to prevent ocular exposure. The modules are housed in compact aluminum cases (90 mm $\times$ 90 mm $\times$ 45 mm) equipped with two-way adjustable pitching platforms, allowing precise angular adjustments within $\pm 0.5^\circ$ [19]. This flexibility enables the lasers to be oriented horizontally, vertically, or obliquely, depending on the experimental setup. The lasers are arranged in a 3 $\times$ 6 vertical matrix, forming a structured light curtain that covers a floor area of approximately 1.0 m $\times$ 0.8 m. The horizontal spacing between adjacent laser beams is set at 0.2 m, providing a high horizontal resolution that allows the system to capture fine-scale spatial variations in $PM_{2.5}$ concentrations (Figure 2) [19]. The vertical coverage extends up to 2.2 m, encompassing the typical human breathing zone and enabling the detection of vertical concentration gradients. Each laser beam has a width of approximately 7 mm at the observation point,

ensuring minimal interference between adjacent beams and maintaining clarity in the captured images [19].

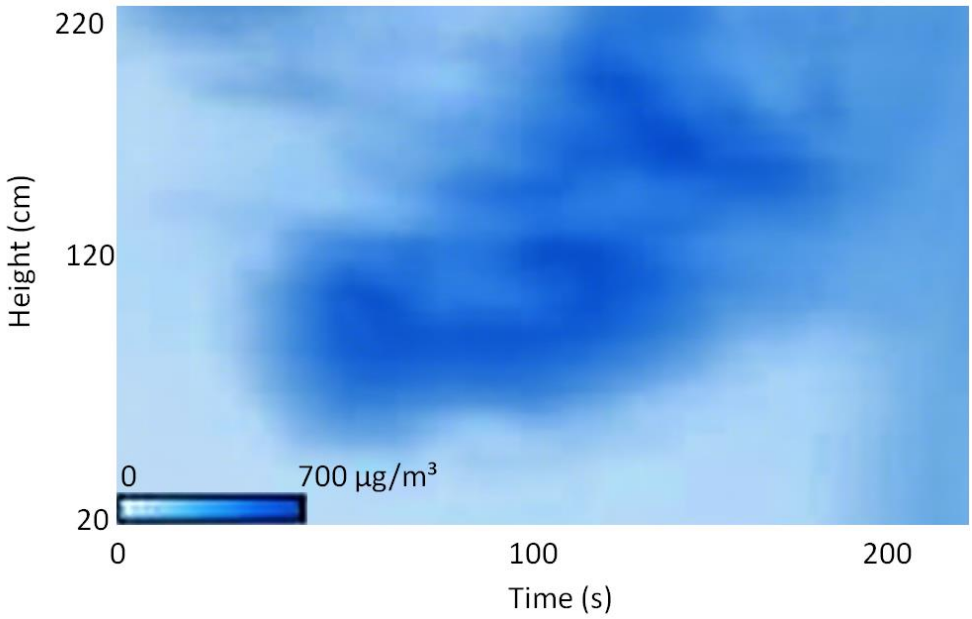


Figure 2. Vertical $PM_{2.5}$ profiles during incense burning were dynamically measured using a calibrated 3D I-LiDAR along a single beam (length: 220 cm), with concurrent sensor validation at the test site corner. Darker color indicates higher concentration. (He et al., 2022; Copyright 2022 American Chemical Society) [19].

The imaging system utilizes a high-resolution monochrome CMOS camera (MV-CH089-10GM) with a sensor resolution of 4104 × 3006 pixels [19]. To enhance sensitivity and reduce noise, the operational resolution is set to 1026 × 750 pixels by binning pixels in a 4 × 4 configuration. The camera is equipped with a 16 mm focal length lens, providing a wide field-of-view of 107°, which is essential for capturing the entire laser array within a confined indoor space. A critical component of the imaging system is the use of a 532 nm narrow-band optical filter, which selectively transmits the laser wavelength while rejecting ambient light, significantly improving the signal-to-noise ratio [30]. Additionally, a light-absorbing backdrop is employed to minimize background reflections and further enhance image quality. The camera operates at a frame rate of 10 frames per second (fps), enabling real-time monitoring of dynamic processes such as plume formation and dispersion [28]. This temporal resolution is sufficient to capture most indoor air movement phenomena, which typically occur on timescales of seconds to minutes [19,23].

The calibration model converts grayscale values into $PM_{2.5}$concentrations using a multi-parameter empirical equation [19]. After simplification based on experimental data, the final model is expressed as a linear function of light intensity (I) and attenuation (A). Detailed derivation and full equations are provided in the Supplementary Information. The concentration retrieval is based on several key assumptions: (1) aerosols are homogeneous spherical particles following Mie scattering theory; (2) attenuation along the laser path is primarily caused by $PM_{2.5}$, with gas absorption considered negligible; and (3) ambient light interference is sufficiently suppressed by the narrow-band optical filter. Major sources of uncertainty and their associated impacts are as follows: Aerosol properties, such as variations in particle size distribution (e.g., smoke versus dust), influence the scattering phase function and alter the relationship between grayscale and concentration. Chemical composition, especially

hygroscopicity, can cause overestimation under high relative humidity conditions. Signal saturation occurs in both the CMOS camera and reference PM sensors at concentrations above 500 $\mu g/m^3$, leading to underestimation, while significant uncorrected multiple scattering effects are expected beyond approximately 1000 $\mu g/m^3$, making data above this concentration unreliable. Environmental robustness is affected by ambient lighting variations, which are partially mitigated by optical filters, though strong direct light may still cause interference [19]. Differences in wall or surface reflectance are corrected via background subtraction, but occlusions caused by moving objects such as people or doors result in data gaps that require multi-angle setups or spatial interpolation to address. System stability is maintained by controlling laser power drift (under 5% per hour) and frame-to-frame misalignment (below 1 pixel) through periodic background frame calibration. In terms of laser safety, Class IIIB lasers (wavelength 532 nm, power 130–160 mW) require strict safety protocols. Deployment must prevent direct eye exposure to the beam by installing at heights above 2 m, using physical enclosures or barriers, and posting clear warning labels. The maximum permissible exposure for skin or eyes is 0.25 s, necessitating measures to avoid prolonged exposure. The calibration model for the 3D I-LiDAR system was validated using 21,543 data pairs, with 80% used for training and 20% for testing. The normalized mean bias (NMB) ranged from −0.05 to 0.03, and the normalized mean error (NME) from 0.07 to 0.16, indicating high accuracy and robustness across all 18 laser units [19]. This large-scale validation underscores the reliability of the system under controlled indoor conditions. Therefore, the system is best suited for concentrations below this threshold, which covers most typical indoor scenarios. The 3D I-LiDAR system has been successfully deployed to monitor $PM_{2.5}$ emissions from cigarette smoking and incense burning. In the case of cigarette smoking, the system captured the rapid upward movement of $PM_{2.5}$ due to thermal buoyancy, with plumes reaching heights exceeding 2 m within seconds [19]. The data revealed significant turbulence and irregular fluctuations at plume boundaries, attributed to human exhalation and indoor air currents. In contrast, incense burning produced a steadier, slower-rising plume with a well-defined boundary, reaching 220 cm over 800 s with a stable vertical gradient. The system's ability to generate real-time 3D concentration animations provides unprecedented insight into pollutant behavior, including emission rates, dispersion patterns, and mixing processes [19]. The high spatiotemporal resolution allows researchers to identify transient events and small-scale gradients that are invisible to traditional point sensors. The 3D I-LiDAR system offers advantages such as non-intrusive measurement, true 3D dynamic monitoring, and high spatiotemporal resolution (0.2 m horizontally, 2.2 m vertically, 10 fps), enabling accurate visualization of pollutant dispersion processes. However, it also has limitations including signal saturation at high concentrations (>500 $\mu g/m^3$), complex calibration with strong environmental dependency, high cost and expertise requirements for operation, and the need for strict protective measures due to the use of Class IIIB lasers [19,28,30]. To comprehensively characterize the system's performance, key operational parameters and uncertainties are summarized in Table 2. While the current empirical model performs robustly under controlled conditions, its accuracy can be influenced by aerosol properties (e.g., size distribution, chemical composition for smoke vs. cooking aerosol) and environmental factors like relative humidity (RH). Future work should integrate RH/temperature sensors and develop multi-variable calibration models to enhance cross-source applicability and minimize related uncertainties.

In recent years, high-resolution monitoring technologies for indoor $PM_{2.5}$have evolved from traditional single-point fixed monitoring towards dynamic, multi-

dimensional, and fused sensing approaches. Based on the literature review, current mainstream technologies can be categorized into three types: (1) mobile monitoring systems based on portable sensors; (2) three-dimensional monitoring systems based on optical remote sensing; and (3) hybrid sensor networks. Our analysis has identified several key research gaps, including the lack of standardized calibration protocols for low-cost sensors in multi-source environments, insufficient validation of 3D imaging LiDAR in large or complex indoor spaces, and a disconnect between real-time health data and exposure metrics. Mobile monitoring technology, due to its flexibility and direct reflection of personal exposure, has been widely applied in small-scale environments such as homes and offices [11,23]. In contrast, technologies like 3D I-LiDAR, despite higher costs, provide non-intrusive full-field visualization data, making them suitable for researching pollution source dispersion mechanisms and monitoring large spaces [19,28]. Furthermore, a growing number of studies are beginning to explore multi-technology integration pathways, such as combining mobile monitoring with fixed LiDAR to achieve multi-scale linkage from macroscopic fields to microscopic exposure [23]. These trends indicate that future indoor air quality monitoring will place greater emphasis on data fusion, intelligent calibration, and deep integration with health applications.

Table 2. Performance characteristics of the 3D I-LiDAR system [19].

Parameter	Value/Description	Notes
Measurement Range	3–500 $\mu g/m^3$	Signal saturation occurs beyond ~500 $\mu g/m^3$
Limit of Detection (LOD)	3 $\mu g/m^3$	Based on background noise level
Limit of Quantification (LOQ)	10 $\mu g/m^3$	$R^2 > 0.95$ within this range
Accuracy (NMB)	−0.05 to 0.03	Validated with 21,543 data pairs
Precision (NME)	0.07 to 0.16	Validated with 21,543 data pairs
Linear Range	3–500 $\mu g/m^3$ ($R^2 \geq 0.95$)	Extrapolation or piecewise calibration needed beyond
Inter-unit Variability	<10% (across 18 laser units)	Controlled via unified calibration model
RH/Temperature Impact	Not explicitly quantified in model	Real-time compensation using sensors is recommended
Cross-source Calibration	Specific factors for incense/cigarette smoke	Requires extension to other sources (e.g., cooking, dust)
Drift Control	Relies on periodic background correction	Automatic background sampling every 6 h is advised

3.3. Technology Comparison and Integration Prospects

3.3.1. Fusion Workflow

Mobile monitoring provides accurate data on individual exposure points, while 3D I-LiDAR provides spatiotemporal context of the overall pollution field (Table 3). Their integration can exert synergistic value in three major scenarios. First, 3D I-LiDAR can serve as a verification and calibration benchmark for mobile monitoring. Its high-resolution concentration field can verify the accuracy of interpolation algorithms in mobile monitoring, optimize sensor source-specific calibration factors (e.g., for cooking fumes or smoke), and correct positioning deviations caused by occlusion. Second, integration enables multi-scale connections between environmental concentration and personal exposure. Three-Dimensional I-LiDAR monitors global pollution distribution and migration, while mobile monitoring synchronously tracks individual trajectories and

real-time exposure, jointly revealing the spatial causes of exposure events (e.g., passing through high-concentration areas) and the impact of individual activity patterns. Third, in intelligent building integration, 3D I-LiDAR can be used as fixed infrastructure to achieve zoned pollution monitoring and link with ventilation systems for zone-specific purification; mobile monitoring, through wearable devices that sense personnel location, supports person-specific regulation. The combination of the two can construct a dynamic pollution-personnel-regulation model, ensuring health while reducing energy consumption and realizing accurate, energy-efficient air quality management. In conclusion, the integration of mobile monitoring and 3D I-LiDAR represents the future direction of indoor air quality research. Through the combination of point and field data and multi-scale synergy, it provides a more comprehensive and reliable solution for health exposure assessment and intelligent environmental control.

Table 3. Comparison of mobile monitoring and 3D I-LiDAR technologies for indoor $PM_{2.5}$ monitoring [11,19].

Feature	Mobile Monitoring [11]	3D I-LiDAR Monitoring [19]
Monitoring Paradigm	Lagrangian, human-centered	Eulerian, space-centric
Spatial Dimension	2D trajectory and interpolation plane	True 3D volumetric field
Temporal Resolution	High (1 s)	Very high (up to video frame rate, e.g., 10 frames per second)
Measurement Method	Direct contact measurement (point sampling)	Non-contact remote sensing (line/area scanning)
Core Advantage	Directly reflects personal exposure, high flexibility, relatively low cost	No flow field interference, global visualization, full spatial continuous monitoring
Main Limitation	Path dependency, sensor response delay, may interfere with personnel activities	Signal saturation at high concentrations, complex calibration, expensive equipment, potential laser safety risks
Practical Applicability	Homes, offices, personal exposure tracking	Labs, industrial sites, source dynamics studies
Best Application Scenario	Personal exposure assessment, microenvironment identification, unknown pollution source investigation	Dynamic emission process of pollution sources, turbulence and diffusion mechanism research, 3D dynamic visualization

A practical and reproducible workflow for integrating mobile monitoring and 3D I-LiDAR data begins with data synchronization by aligning the respective datasets using a unified high-precision timestamp. Subsequently, mobile point measurements are spatially interpolated onto a 2D grid via methods such as Kriging or Inverse Distance Weighting to enable direct comparison with horizontal slices of the I-LiDAR 3D field. Personal exposure dose is then calculated by integrating the $PM_{2.5}$ concentration over time along an individual's trajectory, yielding results in units of $\mu g \cdot min/m^3$, where the 3D I-LiDAR data provide crucial context for concentrations in unvisited areas or help correct for mobile sensor delay. Finally, the high-resolution 3D I-LiDAR field serves as a benchmark for validating and refining source-specific calibration factors for the mobile sensors, particularly within hotspot regions identified by the 3D I-LiDAR system.

3.3.2. Worked Case Study

In a simulated scenario within a 30 m^2 apartment during cooking, mobile monitoring detected a peak concentration of 120 $\mu g/m^3$ near the stove [11]. Concurrently, the 3D I-LiDAR visualized the plume's upward dispersion, revealing a strong vertical gradient. Data fusion demonstrated that although the occupant spent only 5 min in the kitchen, this

short exposure in the high-concentration zone contributed to 40% of their total integrated $PM_{2.5}$dose during the monitoring period [19]. This highlights a risk that would be underestimated by mobile data alone if interpolation failed to capture the peak accurately, or would be overestimated if the sensor's slow response time was not accounted for using the dynamic 3D I-LiDAR data. This pipeline is generalizable to any indoor environment equipped with IPS and 3D monitoring capabilities. The specific interpolation algorithm and calibration factors may need adjustment based on space size, pollution source type, and sensor performance [11,19,25–27].

4. Future Research Directions and Challenges

4.1. Intelligent Calibration and Data Processing

Improving monitoring accuracy and system stability is a core challenge [31]. Three-Dimensional I-LiDAR faces problems of low efficiency in processing massive image data and easy misalignment of calibration models in complex environments [28]. In the future, machine learning (e.g., convolutional neural networks) should be introduced to develop efficient image processing models, enabling fast, automatic conversion from light intensity to concentration [32,33]. Meanwhile, adaptive calibration models need to be constructed to real-time compensate for the effects of temperature, humidity, background light changes, and high-concentration nonlinear responses (e.g., sensor saturation) [34,35]. For example, monitoring data under different environments can be used to train algorithms to realize autonomous optimization of calibration parameters. For mobile monitoring, the key lies in multi-source data fusion [32], which integrates multiple sensors (e.g., $PM_{2.5}$, temperature, humidity, and positioning sensors), requiring algorithms such as Kalman filtering and Bayesian estimation to solve issues of time synchronization and accuracy differences, thereby reducing errors from single sensors. Additionally, the spatial concentration reference field provided by 3D I-LiDAR can be used for real-time drift correction of low-cost sensors, extending their effective service life. Based on the literature analysis, we argue that a core bottleneck in current high-resolution monitoring technologies is the lack of generality and adaptability of calibration models. Future work should prioritize developing machine learning-based adaptive calibration algorithms capable of dynamically adjusting model parameters based on environmental factors (e.g., temperature, humidity, background light) to reduce reliance on laboratory calibration. Furthermore, multi-source data fusion techniques (e.g., Kalman filtering, Bayesian estimation) should become standard components of mobile monitoring systems to enhance data reliability [32,34]. We propose that future research could explore a federated learning framework, enabling distributed sensor networks to collaboratively optimize calibration models while preserving data privacy.

4.2. Technology Standardization and Cost Reduction

This is critical for transforming technology from laboratory research to large-scale application [36]. Currently, both types of technologies lack unified standards, hindering their promotion and data comparability [37,38]. Most 3D I-LiDAR systems are custom-built, with variations in the number of laser units, camera parameters, and other specifications [23,28,37]. In the future, efforts should be made to promote their modularization and standardization, clarifying key parameters such as laser wavelength, power, and data format. Meanwhile, low-cost solutions using consumer-grade laser diodes and CMOS cameras should be developed, maintaining accuracy through optimized optical design and algorithms to enable applications in ordinary households and schools [23,28,37]. For mobile monitoring, a unified calibration protocol and quality

certification system for low-cost sensors need to be established, clarifying calibration procedures and performance indicators for different pollution sources (e.g., cooking fumes, dust). Indoor positioning systems (e.g., ultrasonic, UWB) also require standardization to improve compatibility and positioning stability across different systems [24–26]. Future efforts should also address economic feasibility to facilitate broader adoption. This includes developing low-cost versions of 3D I-LiDAR using consumer-grade components, and establishing subsidy or leasing models for mobile monitoring systems in community-based studies.

4.3. Application Verification in Complex Real-World Scenarios

Current research is mostly limited to controlled environments or small residences, and the effectiveness and adaptability of technologies in large-scale, complex scenarios need urgent verification [19,23,32]. In large spaces (e.g., airports, shopping malls), 3D I-LiDAR faces the problem of laser signal attenuation, requiring optimized laser array arrangement (e.g., layered, multi-array collaboration) to expand coverage; mobile monitoring needs to integrate higher-precision positioning technologies such as UWB to address signal occlusion and reduced accuracy. For complex pollution sources (e.g., industrial emissions, mixed particles from multi-person activities), in-depth research is needed on the impact of different particulate components on sensor response characteristics, and calibration models should be optimized. Additionally, the technology can be used to study the outdoor-indoor penetration process. For example, quantifying the contribution of outdoor $PM_{2.5}$ entering indoors through doors and windows to indoor concentrations and human exposure, providing a basis for optimizing prevention and control measures such as fresh air systems.

Beyond indoor air quality assessment, the integration of mobile monitoring and 3D I-LiDAR holds promise for outdoor environmental research. These technologies can be deployed to identify and characterize plumes from large stationary anthropogenic sources (e.g., industrial stacks, wildfires) and to pinpoint areas of interest for subsequent detailed analysis using unmanned aerial vehicles (UAVs) equipped with sensors. Such multi-platform approaches offer an affordable and scalable alternative to traditional monitoring methods, enabling high-resolution spatiotemporal mapping of pollution dispersion in complex environments [2,10,14,39–43].

4.4. Deep Integration with Health Research

The ultimate goal of the technology is to support precise health risk assessment [39]. Future work should deeply integrate high-resolution exposure data with epidemiological and toxicological studies to establish quantitative exposure-health effect relationships. Mobile monitoring can track the personal exposure trajectories of specific populations (e.g., children, individuals with respiratory diseases) and, combined with physiological data from wearable devices (e.g., heart rate monitors), analyze the acute health effects of short-term exposure [7,40]. The pollutant dispersion dynamics provided by 3D I-LiDAR can help explain the spatial causes of exposure disparities and identify high-risk microenvironments (e.g., near kitchen stoves, printers). Furthermore, integrating machine learning can help build real-time individual health risk prediction models, enabling a closed loop from exposure warning to personalized health intervention.

4.5. Expansion into Occupational Safety

The integrated technology has broad application prospects in these fields [44,45]. In occupational safety (e.g., mines, construction sites), mobile monitoring can be integrated into safety gear to assess workers' personal exposure doses in real time [44,45]. Meanwhile, 3D I-LiDAR can provide global monitoring of dust dispersion and high-

concentration zone distribution across the entire worksite. Together, they can offer decision support for optimizing workflows, improving ventilation systems, and implementing targeted personal protection, thereby fundamentally reducing the risk of occupational diseases such as pneumoconiosis. Current research predominantly focuses on residential and commercial environments, while applications in industrial, mining, and other high-risk settings remain nascent. We highlight that the integration of mobile monitoring and 3D I-LiDAR holds significant potential for occupational health protection, enabling real-time assessment of worker exposure levels and visualization of dust dispersion pathways to inform ventilation optimization and personal protection strategies [44,45]. Moving forward, it is crucial to develop technical standards and safety protocols tailored for industrial environments to facilitate the transition of these technologies from laboratory research to field application.

5. Conclusions

This study reviews two principal approaches in high-resolution spatiotemporal monitoring of indoor $PM_{2.5}$ including mobile monitoring and three-dimensional imaging LiDAR (3D I-LiDAR), and proposes a synergistic framework combining personal exposure tracking with full-field visualization. Mobile monitoring is human-centered, providing direct individual exposure data, but suffers from response delays and path dependency. Three-Dimensional I-LiDAR enables non-invasive 3D concentration field reconstruction with high spatiotemporal resolution but faces challenges like signal saturation and high costs. Each technology has its own advantages in exposure assessment and dispersion mechanism research, and their integration can achieve multi-scale linkage from macroscopic fields to microscopic exposure. Through a comprehensive analysis of the literature, it proposes a framework for technological integration and future advancement. The key contributions of this work include: (1) clarifying the respective advantages, limitations, and complementary potential of the two technologies across various scenarios; (2) introducing a point-field fusion concept aimed at multi-scale monitoring; and (3) identifying critical directions for future research, such as intelligent calibration, standardization, and deeper integration with health-related applications. This study not only synthesizes existing research but also offers a theoretical foundation and strategic pathway for future technological development and practical implementation. This study provides a novel comparative analysis of Lagrangian (mobile) and Eulerian (3D I-LiDAR) monitoring paradigms for indoor $PM_{2.5}$. By highlighting their complementary strengths and proposing a synergistic framework, we advance the potential for multi-scale exposure assessment and intelligent indoor air quality management. Future work should focus on intelligent calibration, standardization, and real-world integration to bridge the gap between laboratory research and practical application.

In conclusion, mobile monitoring and 3D I-LiDAR each present distinct profiles of advantages and limitations that dictate their optimal applications. Mobile monitoring excels in providing direct personal exposure data with high flexibility and relatively low cost, making it ideal for assessing individual-level exposure in environments like homes and offices; however, its utility is constrained by sensor response delays, path dependency, and potential interference with natural movement, with its future potential lying in integration with wearable health devices and intelligent calibration for real-time exposure management. In contrast, 3D I-LiDAR offers non-intrusive, high-resolution 3D visualization of pollutant dispersion, which is crucial for studying dynamic emission processes and spatial gradients, yet it faces challenges related to signal saturation at high concentrations, complex calibration requirements, and high operational costs, necessitating future advancements focused on

cost reduction, standardization, and machine learning-enhanced calibration to broaden its applicability in complex indoor environments. Ultimately, the integration of both technologies holds significant promise for multi-scale air quality assessment, synergizing personal exposure tracking with full-field visualization to enable more accurate health risk evaluation and intelligent indoor air quality management.

Supplementary Materials: The following supporting information can be downloaded at: https://www.mdpi.com/article/10.3390/atmos16101196/s1, Text S1. Calibration Model Development and Simplification.

Funding: This research received no external funding.

Institutional Review Board Statement: Not applicable.

Informed Consent Statement: Not applicable.

Data Availability Statement: No new data were created or analyzed in this study. Data sharing is not applicable to this article.

Acknowledgments: I acknowledge He et al. (2022) [19] for the data utilized in Figure 1, which was obtained with permission under Copyright (2022) American Chemical Society.

Conflicts of Interest: The author declares no conflicts of interest.

References

1. Gladson, L.A.; Cromar, K.R.; Ghazipura, M.; Knowland, K.E.; Keller, C.A.; Duncan, B. Communicating respiratory health risk among children using a global air quality index. *Environ. Int.* **2022**, *159*, 107023. [CrossRef]
2. Xu, Z.; Li, D.; Liu, Q.; Li, S.; Li, Y.; Li, S.; Bian, Y.; Kan, X.; Wang, Y.; Liu, J. Global, regional, and national burden of neonatal diseases attributable to fine particulate matter air pollution, 1990–2050. *Environ. Int.* **2025**, *202*, 109638. [CrossRef] [PubMed]
3. Yim, S.H.L.; Li, Y.; Huang, T.; Lim, J.T.; Lee, H.F.; Chotirmall, S.H.; Dong, G.H.; Abisheganaden, J.; Wedzicha, J.A.; Schuster, S.C.; et al. Global health impacts of ambient fine particulate pollution associated with climate variability. *Environ. Int.* **2024**, *186*, 108587. [CrossRef]
4. Joshi, D.C.; Negi, P.; Devi, S.; Lohani, H.; Kumar, R.; Gupta, M.; Ming, L.C. Fine particulate matter ($PM_{2.5}$, PM_{10}): A silent catalyst for chronic lung diseases in India; a comprehensive review. *Environ. Chall.* **2025**, *20*, 101215. [CrossRef]
5. Yun, X.; Shen, G.; Shen, H.; Meng, W.; Chen, Y.; Xu, H.; Ren, Y.; Zhong, Q.; Du, W.; Ma, J.; et al. Residential solid fuel emissions contribute significantly to air pollution and associated health impacts in China. *Sci. Adv.* **2020**, *6*, eaba7621. [CrossRef] [PubMed]
6. Zhang, X.; Staimer, N.; Gillen, D.L.; Tjoa, T.; Schauer, J.J.; Shafer, M.M.; Hasheminassab, S.; Pakbin, P.; Vaziri, N.D.; Sioutas, C.; et al. Associations of oxidative stress and inflammatory biomarkers with chemically-characterized air pollutant exposures in an elderly cohort. *Environ. Res.* **2016**, *150*, 306–319. [CrossRef]
7. Zhang, T.; Man, C.L.; Lui, K.H.; Ho, S.S.H.; Qu, L.; Choi, S.W.; Kwok, T.C.Y.; Ward, T.; Ho, K.F. Personal monitoring of exposure to $PM_{2.5}$ and PMcoarse: A panel study of lung function and oxidative stress biomarkers in elderly Hong Kong residents. *J. Hazard. Mater. Adv.* **2025**, *19*, 100803. [CrossRef]
8. Berg, C.D.; Schiller, J.H.; Boffetta, P.; Cai, J.; Connolly, C.; Kerpel-Fronius, A.; Kitts, A.B.; Lam, D.C.L.; Mohan, A.; Myers, R.; et al. Air Pollution and Lung Cancer: A Review by International Association for the Study of Lung Cancer Early Detection and Screening Committee. *J. Thorac. Oncol.* **2023**, *18*, 1277–1289. [CrossRef]
9. Zhang, H.; Evangelopoulos, D.; Wood, D.; Chatzidiakou, L.; Varaden, D.; Quint, J.; de Nazelle, A.; Walton, H.; Katsouyanni, K.; Barratt, B. Estimating exposure to pollutants generated from indoor and outdoor sources within vulnerable populations using personal air quality monitors: A London case study. *Environ. Int.* **2025**, *198*, 109431. [CrossRef]
10. He, J.; Huang, C.-H.; Yuan, N.; Austin, E.; Seto, E.; Novosselov, I. Network of low-cost air quality sensors for monitoring indoor, outdoor, and personal $PM_{2.5}$ exposure in Seattle during the 2020 wildfire season. *Atmos. Environ.* **2022**, *285*, 119244. [CrossRef]
11. Cheng, K.-C.; Tseng, C.-H.; Hildemann, L.M. Using Indoor Positioning and Mobile Sensing for Spatial Exposure and Environmental Characterizations: Pilot Demonstration of $PM_{2.5}$ Mapping. *Environ. Sci. Technol. Lett.* **2019**, *6*, 153–158. [CrossRef]
12. Lu, C.; Xu, H.; Meng, W.; Hou, W.; Zhang, W.; Shen, G.; Cheng, H.; Wang, X.; Wang, X.; Tao, S. A novel model for regional indoor PM2.5 quantification with both external and internal contributions included. *Environ. Int.* **2020**, *145*, 106124. [CrossRef] [PubMed]
13. Wang, B.; Cao, S.; Ma, J.; Huang, N.; Nie, J.; Wang, Z.; Duan, X. 5—Time-Activity Factors Related to Air Exposure. In *Highlights of the Chinese Exposure Factors Handbook (Adults)*; Duan, X., Zhao, X., Wang, B., Chen, Y., Cao, S., Eds.; Academic Press: Cambridge, MA, USA, 2015; pp. 31–39.

14. Steinle, S.; Reis, S.; Sabel, C.E. Quantifying human exposure to air pollution—Moving from static monitoring to spatio-temporally resolved personal exposure assessment. *Sci. Total Environ.* **2013**, *443*, 184–193. [CrossRef] [PubMed]
15. Fappiano, L.; Caracci, E.; Iannone, A.; Murru, A.; Avino, P.; Campagna, M.; Buonanno, G.; Stabile, L. Emission rates of particle-bound heavy metals and polycyclic aromatic hydrocarbons in PM fractions from indoor combustion sources. *Build. Environ.* **2024**, *265*, 112033. [CrossRef]
16. Tofful, L.; Canepari, S.; Sargolini, T.; Perrino, C. Indoor air quality in a domestic environment: Combined contribution of indoor and outdoor PM sources. *Build. Environ.* **2021**, *202*, 108050. [CrossRef]
17. Mazzeo, A.; Pfrang, C.; Nasir, Z.A. Towards developing an indoor emissions inventory for the UK: Challenges and future directions. *Environ. Sci. Atmos.* **2024**, *5*, 151–170. [CrossRef]
18. Liu, Q.; Liu, Y.; Zhang, M. Personal exposure and source characteristics of carbonyl compounds and BTEXs within homes in Beijing, China. *Build. Environ.* **2013**, *61*, 210–216. [CrossRef]
19. He, X.; Zheng, S.; Zhang, H.; Jiao, X.; Cheng, H.; Shen, G.; Tao, S. Three-Dimensional Dynamic Monitoring of Indoor $PM_{2.5}$ with 3D I-LiDAR. *Environ. Sci. Technol. Lett.* **2022**, *9*, 533–537. [CrossRef]
20. Relvas, H.; Lopes, D.; Armengol, J.M. Empowering communities: Advancements in air quality monitoring and citizen engagement. *Urban Clim.* **2025**, *60*, 102344. [CrossRef]
21. Ameen, A.; Rashid, F.L.; Al-Obaidi, M.A.; Bouabidi, A.; Agyekum, E.B.; Chibani, A.; Kezzar, M. A review of impinging jet ventilation for indoor environment control. *Int. J. Thermofluids* **2025**, *29*, 101384. [CrossRef]
22. Zhang, Q.; Li, L.; Zhou, J.; Braham, W.W.; Ma, N. A spatial analysis of ozone and $PM_{2.5}$ distribution for assessing design factors of healthy buildings. *J. Build. Eng.* **2024**, *89*, 109357. [CrossRef]
23. Hu, X.; Assaad, R.H. A BIM-enabled digital twin framework for real-time indoor environment monitoring and visualization by integrating autonomous robotics, LiDAR-based 3D mobile mapping, IoT sensing, and indoor positioning technologies. *J. Build. Eng.* **2024**, *86*, 108901. [CrossRef]
24. Brena, R.F.; García-Vázquez, J.P.; Galván-Tejada, C.E.; Muñoz-Rodriguez, D.; Vargas-Rosales, C.; Fangmeyer, J., Jr. Evolution of Indoor Positioning Technologies: A Survey. *J. Sens.* **2017**, *2017*, 2630413. [CrossRef]
25. Austin, E.; Novosselov, I.; Seto, E.; Yost, M.G. Laboratory Evaluation of the Shinyei PPD42NS Low-Cost Particulate Matter Sensor. *PLoS ONE* **2015**, *10*, e0137789.
26. Kelly, K.E.; Whitaker, J.; Petty, A.; Widmer, C.; Dybwad, A.; Sleeth, D.; Martin, R.; Butterfield, A. Ambient and laboratory evaluation of a low-cost particulate matter sensor. *Environ. Pollut.* **2017**, *221*, 491–500. [CrossRef]
27. Zikova, N.; Hopke, P.K.; Ferro, A.R. Evaluation of new low-cost particle monitors for $PM_{2.5}$ concentrations measurements. *J. Aerosol Sci.* **2017**, *105*, 24–34. [CrossRef]
28. Lim, H.; Chang, H.; Choi, J.B.; Yeum, C.M. LiDAR-3DGS: LiDAR reinforcement for multimodal initialization of 3D Gaussian Splats. *Comput. Graph.* **2025**, *132*, 104293. [CrossRef]
29. Nguyen, L.N.; Susarla, P.; Mukherjee, A.; Cañellas, M.L.; Casado, C.Á.; Wu, X.; Silvén, O.; Jayagopi, D.B.; López, M.B. Non-contact multimodal indoor human monitoring systems: A survey. *Inf. Fusion* **2024**, *110*, 102457. [CrossRef]
30. Liu, J.; Yang, Z.-H.; Tian, Y.-F.; Zhao, Z.-H.; Dong, Z.-Y.; Liu, B.-L.; Yang, Y.-G.; Li, M.-F.; Yu, Y.-J. Dual-wavelength 3D single-pixel imaging based on gated photon counting. *Opt. Lasers Eng.* **2025**, *195*, 109269. [CrossRef]
31. Sá, J.P.; Alvim-Ferraz, M.C.M.; Martins, F.G.; Sousa, S.I.V. Application of the low-cost sensing technology for indoor air quality monitoring: A review. *Environ. Technol. Innov.* **2022**, *28*, 102551. [CrossRef]
32. Tang, Z.; Zhao, Y.; Wang, L.; Tang, J.; Li, G.; Ma, J.; Gao, H.; Huang, T.; Mao, X. A novel approach combining indoor mobile measurements and interpretable machine learning to unveil highly-resolved indoor air pollution. *Build. Environ.* **2025**, *270*, 112552. [CrossRef]
33. Shirowzhan, S.; Sepasgozar, S.M.E.; Li, H.; Trinder, J.; Tang, P. Comparative analysis of machine learning and point-based algorithms for detecting 3D changes in buildings over time using bi-temporal LiDAR data. *Autom. Constr.* **2019**, *105*, 102841. [CrossRef]
34. Butt, F.A.; Jalil, M.; Liaquat, S.; Alawsh, S.A.; Naqvi, I.H.; Muzlifah Mahyuddin, N.; Muqaibel, A.H. Self-calibration of wireless sensor networks using adaptive filtering techniques. *Results Eng.* **2025**, *25*, 103775. [CrossRef]
35. Hu, K.; Yan, C.; Ye, J.; Xu, Y.; Zhu, Z.; Gong, Y. Sensor fault diagnosis and calibration techniques in building energy systems: A review and future outlook. *Build. Environ.* **2025**, *269*, 112365. [CrossRef]
36. Zhao, Y.; Li, Z.; Xia, Y.; Jia, Q.; Zhao, L.; Maboudia, R. Advances in micro- and nano-scale resonant mass-sensitive gas sensors: Mechanisms, materials, functionalization and applications. *Sens. Actuators B Chem.* **2025**, *431*, 137415. [CrossRef]
37. Zhang, Y.; Hou, Q.; Sun, J.; Zhou, X.; Zhang, B.; Lu, J.; Liu, F. Multi-scale and collaborative photon processing for 3D imaging through atmospheric obscurants using an array Gm-APD LiDAR. *Opt. Laser Technol.* **2025**, *190*, 113147. [CrossRef]
38. Lin, Y. Tracking Darwin's footprints but with LiDAR for booting up the 3D and even beyond-3D understanding of plant intelligence. *Remote Sens. Environ.* **2024**, *311*, 114246. [CrossRef]

39. Ou, C.; Li, F.; Zhang, J.; Jiang, P.; Li, W.; Kong, S.; Guo, J.; Fan, W.; Zhao, J. Multi-scenario $PM_{2.5}$ distribution and dynamic exposure assessment of university community residents: Development and application of intelligent health risk management system integrated low-cost sensors. *Environ. Int.* **2024**, *185*, 108539. [CrossRef] [PubMed]
40. Habib, C.; Makhoul, A.; Darazi, R.; Couturier, R. Health risk assessment and decision-making for patient monitoring and decision-support using Wireless Body Sensor Networks. *Inf. Fusion* **2019**, *47*, 10–22. [CrossRef]
41. Zhao, Z.; Pang, Y.; Qi, B.; Zhang, C.; Yang, M.; Ye, X. Vertical Profiling of PM1 and PM2.5 Dynamics: UAV-Based Observations in Seasonal Urban Atmosphere. *Atmosphere* **2025**, *16*, 968. [CrossRef]
42. Mora, S.; deSouza, P.; Duarte, F.; Wang, A.; Paul, S.; Berrones, A.; Ratti, C. Air Quality Monitoring in Coal-Centric Cities: A Hybrid Approach. *Sustainability* **2023**, *15*, 12624. [CrossRef]
43. Shikhovtsev, M.Y.; Makarov, M.M.; Aslamov, I.A.; Tyurnev, I.N.; Molozhnikova, Y.V. Application of Modern Low-Cost Sensors for Monitoring of Particle Matter in Temperate Latitudes: An Example from the Southern Baikal Region. *Sustainability* **2025**, *17*, 3585. [CrossRef]
44. Sadeghi, S.; Soltanmohammadlou, N.; Nasirzadeh, F. Applications of wireless sensor networks to improve occupational safety and health in underground mines. *J. Saf. Res.* **2022**, *83*, 8–25. [CrossRef] [PubMed]
45. Adesoji, T.; Pearce, A.; Kleiner, B.; McGinnis, S. Assessing the impact of green building features on the occupational safety and health of construction workers. *J. Saf. Res.* **2025**, *94*, 59–69. [CrossRef] [PubMed]

Disclaimer/Publisher's Note: The statements, opinions and data contained in all publications are solely those of the individual author(s) and contributor(s) and not of MDPI and/or the editor(s). MDPI and/or the editor(s) disclaim responsibility for any injury to people or property resulting from any ideas, methods, instructions or products referred to in the content.